Journal of Applied Fluid Mechanics, Vol. 18, No. 6, pp. 1534-1549, 2025.
Available online at www.jafmonline.net, ISSN 1735-3572, EISSN 1735-3645.
https://doi.org/10.47176/jafm.18.6.3136

Numerical Investigation of Swirl Recovery from a Transonic Propeller with Swirl Recovery Vanes

S. Raviselvam† and V. Parthasarathy

Hindustan Institute of Technology and Science, Chennai, Tamil Nadu, 603103, India

†*Corresponding Author Email: rs.sr0319@hindustanuniv.ac.in*

ABSTRACT

This research investigates the propeller - stator configuration containing eight bladed transonic rotor and a stator with ten blades as Swirl Recovery Vanes (SRVs) in order to improve the efficiency of propeller propulsion systems. By incorporating SRVs behind the propeller, the study aims to decrease rotational kinetic energy losses, ultimately enhancing aerodynamic performance. The primary goal is to reduce swirl, resulting in a 4.46% increase in power coefficient. The approach entails employing potential-based design methodologies in conjunction with time-accurate Reynolds-averaged Navier-Stokes (RANS) simulations. The simulations were validated through comparisons between the numerical and analytical slipstream data. Further enhancement of additional thrust of 23N and improvement in the efficiency of the propeller by 3.47% during cruise phase is achieved. Also, the results indicated a potential increase in the overall propulsive efficiency of the propeller – SRV combination to an extent of up to 3.46%. These improvements are achieved by varying the pitch distribution of the SRVs to enhance swirl recovery. Adjusting the pitch has demonstrated an increase in these gains by enhancing the swirl recovery of the rotor. The flow in the propeller slipstream leads to the emergence of unsteady phenomenon on the vanes. Design modifications to the swirl recovery vanes are deemed necessary for achieving further improvement in these configurations.

Article History

Received September 19, 2024
Revised January 4, 2025
Accepted January 15, 2024
Available online March 30, 2025

Keywords:

Swirl recovery
Propeller – SRV
Pitch distribution
Propulsive Efficiency
Power Coefficient

1. INTRODUCTION

The increasing demand to reduce fuel consumption in civil aviation has led to a renewed focus on propeller propulsion systems. Turboprop engines are particularly noteworthy for their superior propulsive efficiency compared to fan engines of similar technological sophistication, making them an attractive solution for achieving low-emission aircraft propulsion (Lombardi, 2011). One promising design strategy to further enhance the propulsion efficiency of these systems is the use of contra-rotating open rotor (CROR) arrangements. Recent studies have examined the aerodynamic and aeroacoustic effectiveness of standalone CROR configurations using both numerical and experimental methods (International Civil Aviation Organization, 2016; International Air Transport Association, 2018). However, the noise generated by the propeller blades, which lack the casing that typically shields turbofans, remains a significant challenge. Contra-rotating propellers hold potential for mitigating swirl energy loss by using a secondary rotating blade row, which may improve propulsive efficiency by up to 8% during cruise (Strack et al., 1981; Mikkelson et al., 1984). Despite these advantages, the increased noise emissions from the CROR configuration have sparked considerable research, especially concerning semi-installed (ATR, 2018) and fully installed configurations (Beck et al., 2015).

For high-speed transonic cruise, the aerodynamic and aeroacoustic characteristics of propellers impose limitations on the Mach number at the blade tip. The elevated airflow velocity at these speeds necessitates a reduction in rotational velocity, resulting in higher propeller disc loading. This, in turn, leads to increased swirl losses in the propeller slipstream and reduces overall propulsive efficiency (Beaumier, 2012). One approach to mitigate these losses is the incorporation of a second rotating blade row in CROR propellers, which can recover swirl energy and potentially enhance efficiency by up to 8%. Additionally, interactions between the propeller and wing have been shown to reduce lift-induced drag by recovering angular momentum (swirl) through the wing's

trailing flow (Witkowski et al., 1989; Samuelsson, 1990; Stuermer, 2006).

An alternative method to improve propeller efficiency without the added complexity of contra-rotating devices is the use of stationary downstream blades—swirl recovery vanes (SRVs). Wind tunnel experiments have shown that SRVs can significantly improve efficiency by recovering swirl energy, with improvements of up to 2%, without introducing additional noise compared to standard propeller configurations (Veldhuis, 2005). In this regard, the Delft University of Technology has conducted studies employing SRVs as a fixed array of vanes functioning similarly to a stator, achieving efficiency gains without the complications associated with CROR designs (van Kuijk, 2015). NASA's experimental studies on high-speed propellers have also validated these findings, demonstrating a 2% improvement in efficiency (Miller, 1988; Gazzaniga & Rose, 1992). These vanes are designed to recover swirl in the slipstream, thereby producing additional thrust (Dittmar & Hall, 1990). More recent studies have shown that SRVs can boost thrust while enhancing aerodynamic performance, though the impact on overall system efficiency remains a subject of further investigation (Sinnige et al., 2015; Wang et al., 2014). Despite these promising results, the integration of SRVs into propeller systems still requires careful design to balance the potential gains with any negative effects on efficiency.

The research detailed in Stokkermans et al. (2016) focused on a comprehensive study of the influence of pylon blowing on the installation of pusher propellers as part of the APIAN-INF experiment. This study demonstrated the need for further investigation into the integration of SRVs and their effect on propeller efficiency. In light of the scarcity of studies specifically addressing SRVs, the impact of these vanes on the aerodynamic characteristics of propeller propulsion systems remains a largely unresolved area of research. Previous studies, such as those by Yamamoto (1992), Miranda & Brennan (1986), and Kroo (1986), have also explored the aerodynamic benefits of swirl recovery and its influence on propeller performance, further highlighting the importance of optimizing SRV integration for improved propulsion efficiency. Additionally, Hager (1988) and Wang et al. (2014) have demonstrated the potential for efficiency improvements with the integration of SRVs, although their research also points to the necessity of effective design and integration to avoid performance trade-offs.

Stuermer et al. (2014a) have contributed significantly to the body of research on CROR propulsion systems, specifically focusing on integrating these systems aerodynamically and aero acoustically to improve efficiency. Their work highlights how the integration of CROR systems could reduce fuel consumption while minimizing noise, which is a key challenge in aviation. In their 2014 paper on the multidisciplinary analysis of CROR systems, they explored the integration of aerodynamics, aeroacoustics, and other engineering disciplines to optimize these propulsion systems for future aircraft, contributing to a better understanding of how CROR configurations can enhance efficiency and reduce noise (Stuermer et al., 2014b). Additionally, their work on low-speed flight conditions validated the performance of CROR systems under specific operational circumstances, ensuring the effectiveness of computational models and experimental findings (Stuermer et al., 2014c). More recently, Stuermer et al. (2022) have expanded this scope, analyzing boundary layer ingesting aft-propulsors to improve aircraft efficiency during cruise conditions. These findings, which focus on drag reduction and fuel efficiency, provide important insights into novel propulsion configurations that could complement or serve as alternatives to traditional CROR designs.

This paper explores the impact of swirl recovery vanes on the performance of propeller propulsion systems. In particular, it investigates the aerodynamic characteristics of a contemporary high-speed rotor, both with and without SRVs downstream. The numerical investigation focuses on SRV blade design and pitch distribution by analyzing the associated flow dynamics using transient RANS analysis. Firstly, the isolated SR3 propeller is analyzed followed by the analysis of propeller – SRV combination. Detailed analysis of the velocity distribution and the swirl indicate an increase in the propeller performance for higher pitch of the stator vanes.

2. ISOLATED SR3 PROPELLER ANALYSIS

Santhi and Vasanthakumar (2022) carried out a computational evaluation of an independent propeller, SR3, running at 6350 rpm. Table 1 shows the comparison of computational values from this study with that of the experimental values of Rohrbach et al. (1982). As seen from the table, optimal efficiency can be adequately estimated, with the Power Coefficient (C_P) and Advance ratio (J) highlighted as critical factors affecting efficiency. In terms of experimental verification, Rohrbach et al. (1982) stress that the accuracy of the experimental data is within one-percent margin, affirming the dependability and accuracy of the SR3 propeller's performance, aligning closely with established experimental standards.

Table 1 Performance parameters of SR3 propeller

Parameter	Computed Values (Santhi & Vasanthakumar, 2022)	Experimental Data (Rohrbach et al., 1982)
Flight Mach, M	0.8	0.8
Efficiency, η	79.8%	80%
Advance Ratio, J	3.6	3.6
Power Coefficient, C_p	1.8	1.8
Pitch, β	63.3°	63.3°

The numerical investigation is carried out using URANS solver of the commercial ANSYS® CFX. focused on the SR3 rotor operating at 35,000 feet altitude with transonic speed. The study consistently produced coherent results in both power coefficient and efficiency. These computed propeller performance characteristics were in good agreement with the experimental findings of Rohrbach et al. (1982). Analysis of the propeller wake parameters, such as axial velocity, tangential velocity, swirl angle, total pressure ratio and static pressure ratio, revealed that these parameters are most prominent at the mid-span of the propeller compared to values at the bottom and tip of the rotor blades. This observation offers valuable insights into the aerodynamic behavior of the SR3 rotor, emphasizing the importance of mid-span conditions in shaping the wake characteristics of the propeller. The outcomes of the computational investigation of SR3 performance closely align with experimental findings, meeting the precision standards set by Stefko & Jeracki (1985).

The main emphasis of this current study is on analyzing the interaction between rotor blades and swirl recovery vanes, highlighting the increased significance of understanding wake dynamics over achieving accurate propeller results. Further, a meticulous volume refinement strategy is applied in the wake region behind the propeller. This refinement approach aims to improve the precision of simulations, particularly in critical areas essential for comprehending wake characteristics, thus facilitating a more thorough examination of the interaction between rotor blades and swirl recovery vanes.

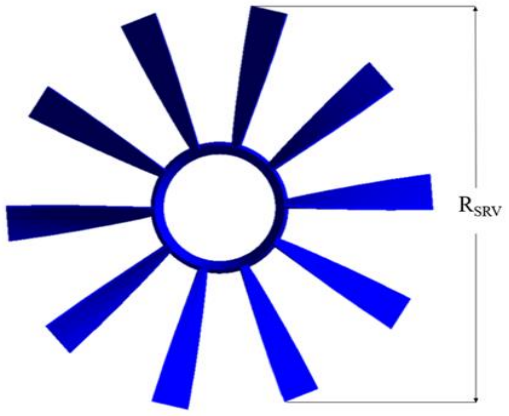

Fig. 1 Layout of swirl recovery vanes

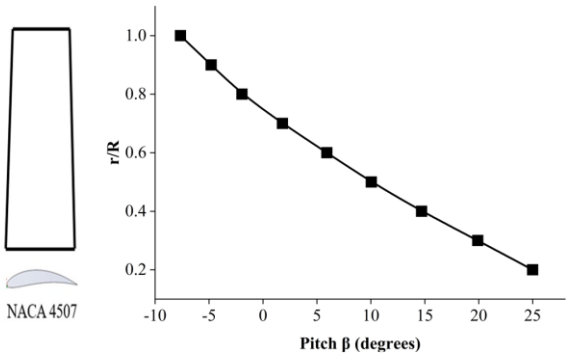

Fig. 2 Design of SRV chord at pitch of 5º with airfoil section.

3. PROPELLER – SRV ANALYSIS

3.1 SRV Design Procedure

This section outlines the layout of the SRV as depicted in Fig. 1, including the planform, for the pitch angle of 5º, and airfoil section illustrated in Fig. 2.

In the quest to minimize aerodynamic interference-induced swirl, the layout integrates eight vanes, matching the quantity of rotor blades. The stator layout is optimized for four distinct cases, featuring angles of 0º, 5º, and 10º in comparison to the rotor with an airfoil profile. Importantly, asymmetrical airfoils are favored for the stator design to enhance overall performance. For scenarios requiring higher thrust settings, the NACA 4507 airfoil, as employed by Stokkermans (2015), is adopted for its high thrust capabilities. This airfoil is utilized across the entire span of the SRV, with its thickness carefully selected to strike a balance between maximizing performance and ensuring structural durability. Furthermore, the stator's tip radius matches that of the propeller at 0.311 meters, contributing to the overall aerodynamic efficiency of the system.

3.2 Domain Geometry

The computational model for the rotor adopts a domain structure similar to the isolated case, divided into three sections: outside, rotatory and wake dimension. The computational domain is similar to the domain used in Ortun et al. (2012). The outer and propeller zones replicate

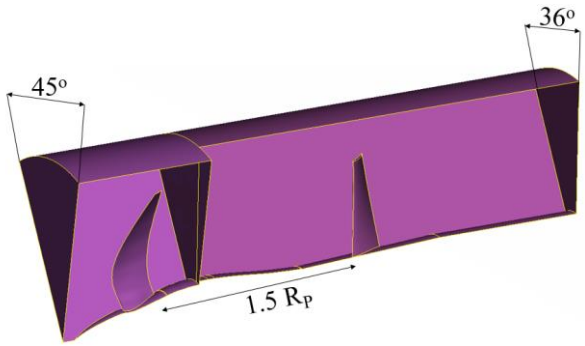

Fig. 3 The propeller-SRV CFD model's rotating and wake zones

those in the isolated propeller CFD approach, comprising a 45˚ wedge with a single SR3 rotor blade, spinner, and hub. Notably, the wake area undergoes slight modification, with one of the vanes positioned at a distance of 1.5R_p downstream of the rotor as depicted in Fig. 3.

This visual representation is crucial for understanding the aerodynamic characteristics of the system and the impact of the SRV on the wake and overall rotor efficiency. Figure 4 offers a schematic view of the system, showcasing the configuration both with and without the swirl recovery vane along the axis of rotation with four planes at 1R_p, 1.35R_p, 2R_p, and 2.4R_p downstream.

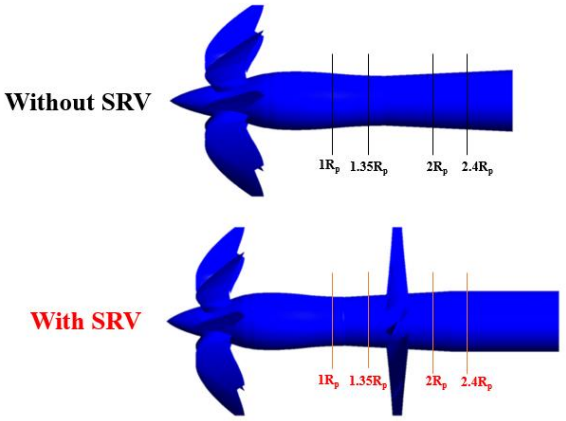

Fig. 4 Schematic view of propeller without and with SRV at four planes downstream of the propeller – SRV at J = 3.6

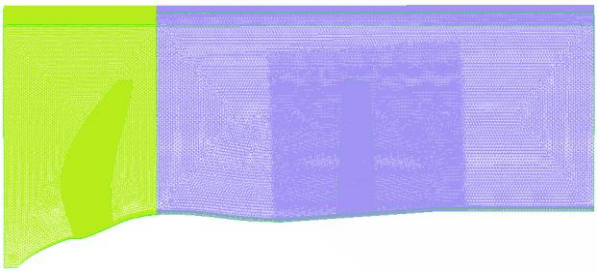

Fig. 5 The propeller-SRV computational grid

3.3 Mesh

Meshing was performed using the ANSA tool. Table 2 provides a detailed examination of the comprehensive mesh characteristics. The non-uniform grid comprises triangular border meshes. The 20-layer structure consists of semi-structured prismatic elements situated along walls with no-slip condition, along with tetrahedral elements distributed throughout the entire domain. Mesh density is controlled through wall refinement on no-slip walls, volumetric refinement in rotational and wake zones, initial film thickness of inflated layers, and a proportional increase in both the inflation layer and total mesh growth.

The initial layer corresponds to a y+ value of 0.5. The total number of inflation layers is precisely adjusted to effectively enclose a boundary over the blade and nacelle. Because of the close proximity of the rotating region to the outer and wake regions, a sliding-mesh approach is employed to facilitate the movement of the rotating region. When investigating mesh dependence, these refinements, along with enhancements in mesh density within the rotating and wake regions, undergo modifications. Figure 5 illustrates the computational grid for the propeller-SRV configuration, offering insights into the distribution of elements within the model. Operating conditions, initial and boundary conditions, solver and turbulence model details are provided in Table 3. High-thrust simulations utilize J = 3.6 to minimize computational expenses. Grid properties and turbulence model employed are similar to the isolated propeller CFD analysis.

Table 2 Illustration of the essential grid selection for the rotor stator flow field

Variable	Value
Category of Meshes	Unstructured
Type of Elements Wall Volume	 Triangular Tetrahedral
Inflation layer Growth rate Element Type First layer Thickness No. of layers	 1.2 Prismatic 0.5 mm 20

Table 3 The initial and boundary conditions for the rotor- stator simulation

Parameter	Value
Flight Mach, M_∞	0.8
Density, ρ_∞	0.3825 Kg/m^3
Freestream velocity, V_∞	237.2448 m/s
Advance Ratio, J	3.6
Total Pressure, P_∞	23842 Pa
Altitude, h	35,000 feet (10668 m)
Speed of sound, a_∞	296.556 m/s
Total temperature, T_∞	218.8 K
Reynolds number, Re_c	7.98×10^5
Dynamic viscosity, μ	1.435×10^{-5} Kg/m. s
Chord length at 3/4th of the blade span, L	0.113204 m
Solver	Unsteady RANS, Second order upwind scheme
Passing Period	0.00923078 s
Turbulence model	SST, k-ω
Rotating Frame	Frozen Rotor
No slip wall	Propeller blade, Propeller hub, stator hub
Free slip wall	Freestream (Outer domain hub and shroud)
Interfaces	Side(2x) rotational periodic boundary condition, Translational periodicity for propeller shroud, Transient rotor stator for interface between rotor & stator

3.4 Mesh Dependency Study

The unsteady computation analysis of the propeller-SRV combination is carried out using URANS solver of the commercial ANSYS® CFX. The mesh dependency is studied for coarse, medium and fine grids. The time averaged axial velocity distributions at various axial locations downstream of the rotor and stator are presented for the coarse, medium and fine meshes. The SRV is located at $1.5R_p$ from the rotor trailing edge (R_p - radius of the propeller); Fig. 4 shows that two planes are chosen downstream of the rotor ($1R_p$ and $1.35R_p$ between rotor

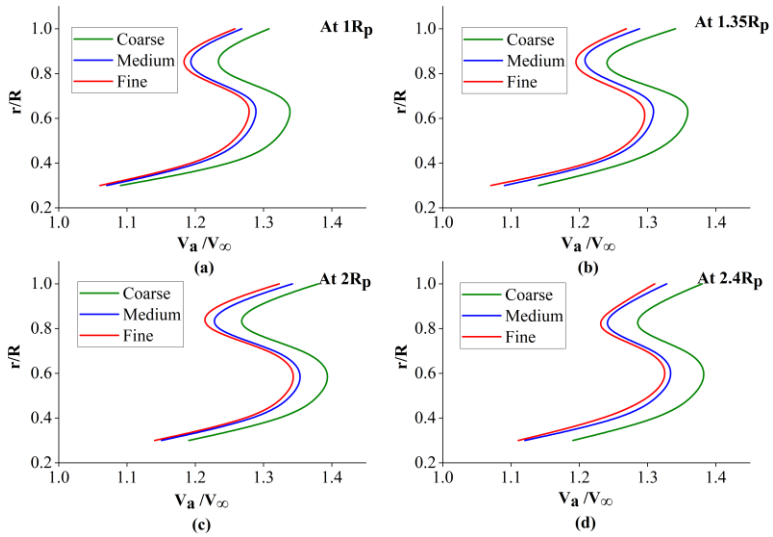

Fig. 6 Radial distribution of axial velocity component downstream of the propeller with a pitch of 0˚ for the coarse, medium and fine mesh

Table 4 Details of grid dependency study of propeller SRV model

Elements	Pitch β	Count (M)	C_Q	C_P	C_T	η %
Coarse	0˚	3.8	0.296	1.861	0.424	82.14
Medium		4.8	0.297	1.866	0.429	82.99
Fine		5.8	0.297	1.864	0.429	83.03
Coarse	5˚	3.8	0.298	1.874	0.430	82.79
Medium		4.8	0.299	1.884	0.434	83.09
Fine		5.8	0.299	1.884	0.434	83.12
Coarse	10˚	3.8	0.299	1.881	0.429	82.15
Medium		4.8	0.299	1.881	0.435	83.33
Fine		5.8	0.300	1.881	0.434	83.04

and stator) and two planes are chosen downstream of the stator ($2R_p$ and $2.4R_p$ distance from the rotor trailing edge).

Downstream of the Rotor ($1R_p$ and $1.35R_p$): The normalized axial velocity profiles are plotted against the normalized radial distance (r/R_p) at different axial positions downstream of the rotor (Fig. 6).

$1R_p$ Distance: At a distance of $1R_p$ downstream of the rotor, the axial velocity typically exhibits a high core region due to the momentum imparted by the rotating blades. As the radial distance increases, the axial velocity rises near the mid-span and tip. Near the hub, the velocity is generally lower.

$1.35R_p$ Distance: At $1.35R_p$, the flow starts to mix and stabilize. The axial velocity profile begins to level out, with more pronounced peaks persisting near the tip span and at 60% of the mid-span.

Downstream of the Stator ($2R_p$ and $2.4R_p$):

$2R_p$ Distance: With the SRV set at a zero-degree pitch and positioned at $1.5R_p$, there is minimal direct impact on axial velocity at $2R_p$. However, its presence disrupts the swirl, leading to a more uniform axial velocity distribution. The profile becomes smoother, showing less variation across the radius.

$2.4R_p$ Distance: Further downstream at $2.4R_p$, the axial velocity profile continues to smooth out, with the flow becoming fully mixed and achieving a nearly uniform distribution. The initial variations caused by the rotor diminish significantly.

When analyzing the flow downstream of both the rotor and the stator, mesh resolution has a significant impact on the axial velocity results. It's evident that the difference between coarse and medium mesh results are up to 10%, while the difference between medium and fine mesh results is within 2% at an r/R_p value of 0.6 across various axial locations. Similar behavior is observed for other pitch angles of 5° and 10°.

The details of the grid independence study are presented in Table 4. The spatial discretization of the computational domain was carried out using unstructured tetrahedral mesh with prism layer elements to resolve boundary layers. The number of prism layers have been chosen in such a way the minimum and maximum value of y+ is always in the range of 0.001 to 1 respectively.

4. RESULTS AND DISCUSSION

Numerical simulations investigate SRVs in tractor propeller set up, focusing on refining SRV configuration. SRVs, positioned in the propeller slipstream, convert swirl

Table 5 Time-averaged performance overall results of the SR-3 propeller with ten SRV's

	Pitch β	Thrust $T_{overall}$(N)	C_T	C_P	η_P %
Ten SRV	0°	275.5	0.42	1.87	82.99
	5°	278.5	0.43	1.88	83.09
	10°	279	0.43	1.88	83.33
Eight SRV	0°	273.1	0.43	1.87	81.98
	5°	273	0.43	1.87	82.03
	10°	274	0.43	1.88	82.05

Table 6 Propeller-SRV CFD Model vs. Isolated propeller: Time-Averaged Rotor Performance (Table 1)

Pitch β	ΔC_{T_p}%	ΔC_T%	ΔC_P%	$\Delta\eta_{P_p}$%	$\Delta\eta_P$%
0°	8.09	7.62	3.59	3.47	3.10
5°	8.22	8.79	4.59	2.76	3.20
10°	8.72	8.99	4.46	3.25	3.46

into thrust, enhancing propulsion efficiency. Three different pitch configurations are investigated. SRVs augment increased axial velocity, reducing tangential velocity and swirl. Simulations predict a 3.47% increase in propulsive efficiency with SRVs at transonic flight conditions, utilizing the k-ω SST turbulence model. Time-averaged performance parameters, as defined by Stokkermans (2015), are detailed in equations (1 - 6).

The increase in propeller thrust coefficient from incorporating Swirl Recovery Vane:

$$\Delta C_{T_p} = \frac{\left((C_{T_P})_A - (C_T)_B\right)}{(C_T)_B} \quad (1)$$

The change in thrust coefficient by incorporating the Swirl Recovery Vane:

$$\Delta C_T = \frac{\left((C_T)_A - (C_T)_B\right)}{(C_T)_B} \quad (2)$$

The increase in the rotor power coefficient attributed to the incorporation of the Swirl Recovery Vane is:

$$\Delta C_P = \frac{\left((C_P)_A - (C_P)_B\right)}{(C_P)_B} \quad (3)$$

The overall improvement in propeller propulsive efficiency achieved by integrating the Swirl Recovery Vane is:

$$\Delta\eta_{P_p} = J\left(\left(\frac{C_{T_P}}{C_P}\right)_A - \left(\frac{C_T}{C_P}\right)_B\right) \quad (4)$$

Addition of SRV increases overall propulsive efficiency:

$$\Delta\eta_P = J\left(\left(\frac{C_T}{C_P}\right)_A - \left(\frac{C_T}{C_P}\right)_B\right) \quad (5)$$

$$T_{Overall} = \rho_\infty n^2 D^4 \; C_{T_{overall}} \quad (6)$$

Where, A= Propeller +SRV

B= Isolated propeller alone

The outcomes in Tables 5 and 6 are examined below, focusing on the impact of profile transformation. Comparison of SRV slipstream data with that of an isolated propeller. The influence of SRVs on propeller performance are discussed below.

The study aims to enhance single-rotating propellers' efficiency by analyzing propeller SRVs, summarized in Tables 5 and 6. Table 5 shows time-averaged performance with varied pitch angles. In contrast, Table 6 compares SRV outcomes with the baseline (isolated propeller) across five performance metrics.

Using ten SRV blades, a 15° pitch angle for SRV was not feasible because the SRV sector was limited to 36°. This pitch angle would cause the blades to extend beyond the design domain, leaving insufficient space for a 15° configuration. Therefore, further cases with higher pitch angles were not investigated.

Increasing Pitch Angle: Efficiency generally increases with pitch angle due to more effective swirl recovery. Therefore, excessive pitch angles (such as 10°) introduce more flow deflection, increasing the overall efficiency compared to lower pitch angles.

4.1 Propeller - SRV Slipstream Analysis

The research paper explores the integration of a SRV into a propeller system, investigating its effects on propeller performance and emphasizing the importance of SRV positioning. The paper underscores the importance of SRV, necessitating adjustments in vane pitch for optimal performance. Upon aligning vane pitch, the research elucidates the restoration of propulsive efficiency gains linked with the SRV. Moreover, the paper discusses optimizing pitch angle distribution to curtail vane tip losses and reduce induced drag, resulting in notable thrust enhancements.

Drawing attention to SRV installation positions, the research identifies placements based on axial orientations relative to the propeller. Favoring downstream positioning on the blade-down going side, the study reveals superior performance outcomes. Emphasizing the importance of selecting SRV locations where angular velocity is augmented for enhanced thrust generation. Furthermore, a comprehensive parameter study scrutinizes the impact of pitch and blade count variations on SRV efficiency. Therefore, the research underscores the imperative SRV

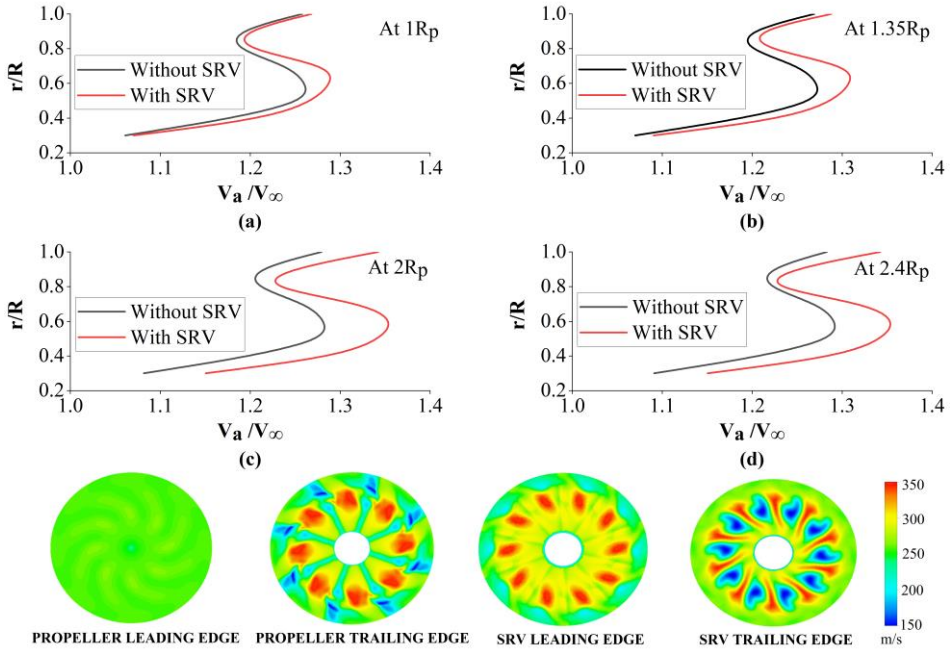

Fig. 7 Radial Distribution and Profile Transformation of Axial Velocity at 0° SRV Pitch

adjustment and positioning to amplify propeller performance.

Downstream Velocity Distribution of Propeller – SRV Configuration

The study analyses circumferentially averaged parameters downstream of a propeller at J = 3.6 in four planes, examining axial, tangential and swirl angle. Red lines denote data with SRV, while black lines represent data without SRV. Initially focusing on the propeller without SRV, simulations were validated using experimental data. SRVs presence leads to inflow from the propeller due to the velocity field generated by the prop's load on the SRV, resulting in time-varying loading on propeller blades. Time-averaged propeller thrust and power significantly differ from the isolated propeller case, as shown in Table 6.

A detailed explanation of how axial velocity, tangential velocity and swirl angle behave at 0°, $5^{\circ}$and 10° pitch across the four planes, with and without SRVs, and how the efficiency increases with various pitch angle.

Axial Velocity

Case 1: SRV at a Pitch = 0°

The axial velocity variations in a propeller-SRV configuration with the SRV at 0° pitch angle provides essential insights into how the SRV affects flow dynamics and enhances propulsion system efficiency. Axial velocity, which represents the flow component along the thrust axis, varies across different planes and radial locations. This variation is fundamental in assessing the overall performance, particularly the flow at key planes: two planes downstream of the propeller (at $1R_p$ and $1.35R_p$) and two planes downstream of the SRV (near the trailing edge at $2R_p$ and further downstream at $2.4R_p$). Figure 7 presents the time averaged axial velocity distribution at the four axial planes of $1R_p$, $1.35R_p$, $2R_p$ and $2.4R_p$ plotted against the normalized radial locations for SRV at 0° pitch. Additionally, the profile transformation contours for axial velocity at the propeller's leading edge & trailing edge, SRV's leading edge & trailing edge, are also shown. The propeller leading-edge plane is positioned $0.75R_p$ upstream of the propeller, while the propeller trailing-edge plane is located $1R_p$ downstream of it. The SRV leading-edge plane is set at $1.35R_p$ downstream of the propeller, and the SRV trailing-edge plane is positioned at $2R_p$ downstream of the propeller.

From Fig. 7, with the SRV at a 0° pitch angle, the transformation of the swirling flow to axial motion is minimal, and the axial velocity shows the least improvement compared to the 5° and 10° pitch cases. Upstream, at $1R_p$, the axial velocity remains low, dominated by the tangential energy imparted by the propeller. At $1.35R_p$, the axial velocity increases slightly due to the thrust generated by the propeller, but the effect is less pronounced due to the persistent swirl. The SRV at 0° pitch does little to reduce the swirl, so the increase in axial velocity between $1R_p$ and $1.35R_p$ is modest, around 2-3%.

Downstream at $2R_p$, the axial velocity shows a minimal increase of only 4-6%. The SRV at 0° pitch has almost no impact on redirecting the tangential energy into axial flow, meaning the flow remains relatively swirl-dominated. The axial velocity profile at $2R_p$ is still somewhat uneven, with noticeable variations across the span. At $2.4R_p$, the axial velocity continues to increase but only by about 6-8%. This minimal increase reflects the SRV's limited ability to affect the flow, as the tangential motion is only weakly converted into axial flow at this pitch angle.

The profile transformation contours for axial velocity at the critical locations reveal that at the SRV's leading edge, the flow retains much of the swirl. As the air moves through the SRV blades, the flow undergoes minimal

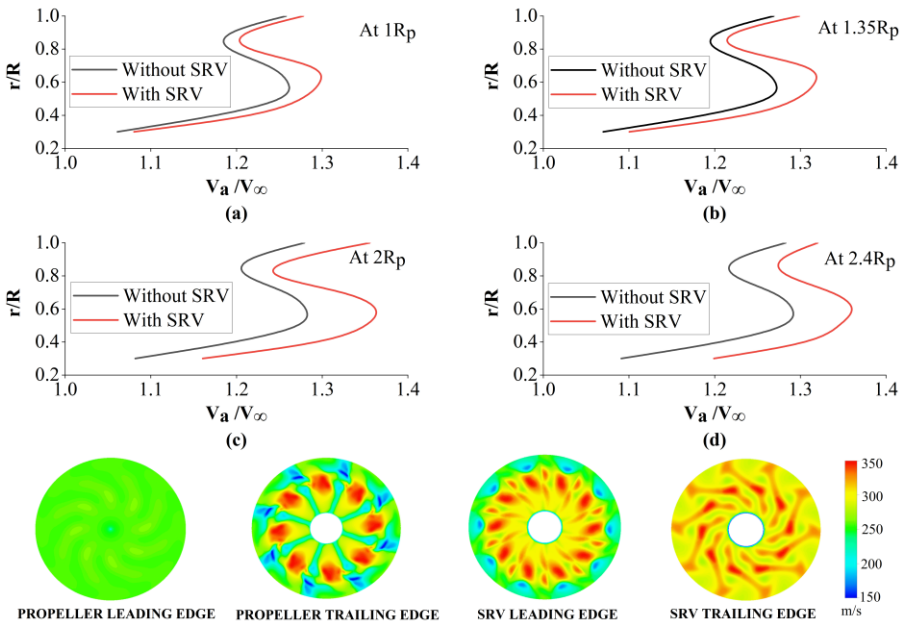

Fig. 8 Radial Distribution and Profile Transformation of Axial Velocity at 5° SRV Pitch

transformation, and by the time it reaches the SRV trailing edge, the axial velocity has increased only slightly. This weak transformation highlights the inefficiency of the 0° SRV pitch in recovering the tangential energy and redirecting it into axial kinetic energy, resulting in a relatively non-uniform flow downstream.

Case 2: SRV at a Pitch = 5°

From Fig. 8, at a 5° pitch angle, the SRV's ability to transform the swirling flow into more uniform axial motion remains effective, though to a slightly lesser extent than at 10°. The axial velocity in the propeller-SRV configuration follows a similar trend, but the magnitude of change is reduced. Upstream, at $1R_p$ (one propeller radius downstream from the rotor), the flow still exhibits a mix of axial and tangential components, with a lower axial velocity due to the swirl-induced by the propeller. As the flow moves to the propeller's trailing edge at $1.35R_p$, the axial velocity increases but remains uneven, as the propeller has not yet fully converted the swirl into axial motion. With the introduction of the SRV at 5°, there is still a noticeable improvement in axial velocity, increasing by about 3-5%, as the SRV partially reduces the swirl, redirecting the flow towards the axial direction. The pitch angle of 5° allows for some recovery of tangential energy into axial energy, although the transformation is not as efficient as with a 10° pitch.

Downstream of the SRV, particularly near the SRV trailing edge at $2R_p$, the axial velocity shows a moderate increase compared to upstream. At this plane, the SRV's effect on reducing the tangential component and redirecting the flow is still significant, but less pronounced than at 10°. The axial velocity at $2R_p$ increases by around 10-12%, reflecting the SRV's ability to recover some of the tangential energy. As the flow moves to $2.4R_p$, the axial velocity continues to increase, but the change is smaller—around 14-16%. The 5° SRV pitch angle does not fully convert all tangential energy to axial energy, and the flow profile at $2.4R_p$ is still somewhat less uniform than at 10°.

The profile transformation contours at critical locations show that, while the flow becomes more axial downstream of the SRV, there is still residual tangential motion. At the SRV's leading edge, the swirl is partially reduced, but not entirely. By the time the flow reaches the SRV's trailing edge, there is a noticeable increase in axial velocity, though with a slightly less uniform profile than at higher pitch angles. The conversion of tangential to axial energy is less efficient at 5°, but the improvement in flow uniformity still contributes to the overall system performance.

Case 3: SRV at a Pitch = 10°

Figure 9 presents the time averaged axial velocity distribution at the four axial planes for the normalized radial locations for the ten-degree pitch. Additionally, the profile transformation contours for axial velocity at the propeller's leading edge & trailing edge, SRV's leading edge & trailing edge, are also shown.

Upstream Flow Dynamics

Upstream of the SRV (downstream of the propeller), the axial velocity exhibits distinct variations as the flow approaches the propeller. At the plane near the rotor at $1R_p$ (one propeller radius downstream of the propeller), the axial velocity is relatively low, as the propeller is just beginning to accelerate the flow. This region is dominated by the rotational energy imparted by the propeller blades, creating a swirl in the flow, with an initial mix of axial and tangential components. As we move to the propeller trailing edge at $1.35R_p$ (1.35 radii downstream from the rotor), the tangential velocity decreases, and the axial velocity gradually rises due to the thrust generated by the propeller. However, the flow remains somewhat uneven and swirl-dominated at this stage, with the axial velocity still in the process of building up. This non-uniform axial

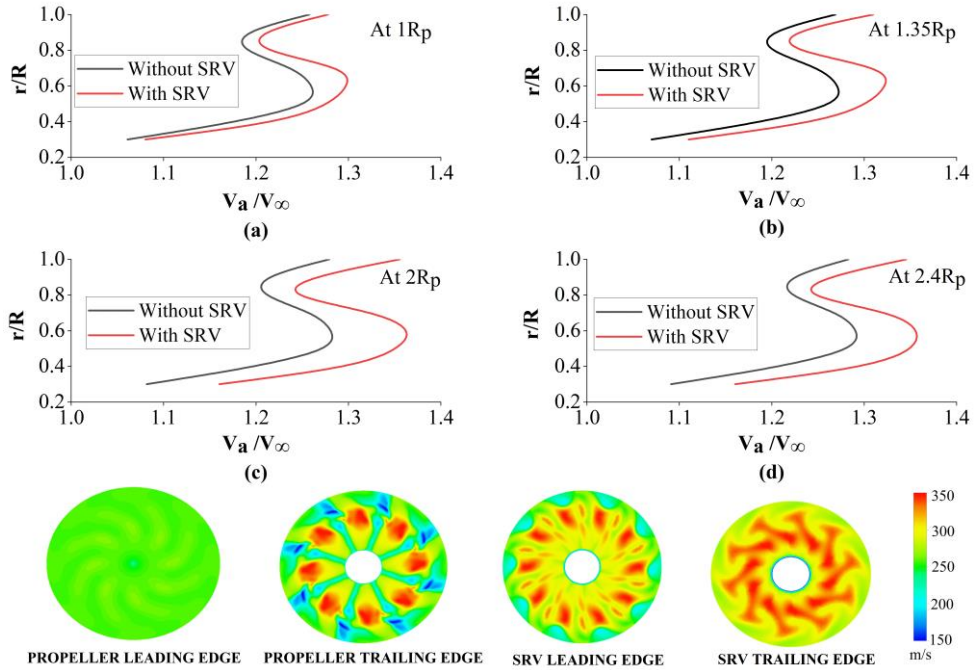

Fig. 9 Radial Distribution and Profile Transformation of Axial Velocity at 10° SRV Pitch

velocity profile upstream is the result of the complex interaction between the rotor's induced swirling flow and the surrounding air. With the introduction of the SRV, the axial velocity at $1R_p$ to $1.35R_p$ increases by approximately 5-7%, as the SRV helps reduce the swirling flow, redirecting it towards more uniform axial motion.

Downstream Flow Transformation

Downstream of the SRV, particularly near the SRV's trailing edge at $2R_p$ (two propeller radii downstream from the rotor trailing edge), the flow undergoes significant transformation. The SRV blades, particularly with the 10° pitch angle, efficiently convert the tangential energy from the swirling flow into axial kinetic energy. As a result, there is a noticeable increase in axial velocity. The axial velocity at $2R_p$ is higher than at the upstream planes due to the SRV's ability to reduce swirl and redirect the flow in the axial direction. The SRV enhances the axial velocity by around 15-18% compared to the baseline case (without SRV), particularly near the trailing edge of the SRV ($2R_p$), where the tangential to axial conversion is most efficient. Moving further downstream to $2.4R_p$ (2.4 radii downstream), the axial velocity profile becomes more uniform and smoother. The SRV's 10° pitch angle ensures a more effective recovery of tangential flow, leading to a steady and higher axial velocity across the span, especially when compared to cases with lower SRV pitch angles. The axial velocity at $2.4R_p$ increases by approximately 20-22%, reflecting the cumulative impact of the SRV in optimizing the flow.

Profile Transformation Contours

The profile transformation contours for axial velocity at different key locations reveal the flow dynamics at various stages. At the angle in recovering tangential energy and converting it into axial kinetic energy. This results in a smoother, more uniform flow, which is crucial for improving the overall efficiency of the system.

Tangential Velocity

Case 1: SRV at a Pitch = 0°

Figure 10 presents the time averaged tangential velocity distribution at the four axial planes of $1R_p$, $1.35R_p$, $2R_p$ and $2.4R_p$ plotted against the normalized radial locations. Additionally, the profile transformation contours for tangential velocity at the propeller's leading edge & trailing edge, SRV's leading edge & trailing edge, are also shown. When the SRV set at a 0° pitch angle, the tangential velocity experiences the least reduction. Upstream at $1R_p$, the tangential velocity is high due to the swirling flow induced by the propeller.

The SRV at 0° pitch does not effectively alter the flow direction, so the tangential component remains dominant. At $1.35R_p$, the tangential velocity shows only a slight decrease, around 3-5%, as the SRV blades make minimal impact on redirecting the swirl into axial motion.

Downstream, near the SRV's trailing edge at $2R_p$, the tangential velocity remains relatively high at the blade tip, with only a modest decrease of about 5-8%. The SRV at 0° pitch does not facilitate the conversion of tangential energy into axial motion effectively, so the flow remains mostly tangential. At $2.4R_p$, the tangential velocity continues to decrease slightly, by around 6-9%, but the reduction is minimal compared to the 5° and 10° pitch cases. This highlights the inefficiency of the 0° pitch SRV in mitigating the swirl and redirecting the flow.

Case 2: SRV at a Pitch = 5°

From Fig. 11, at a 5° pitch angle, the SRV still reduces tangential velocity, but the magnitude of change is smaller compared to the 10° case. Upstream, at $1R_p$, the flow

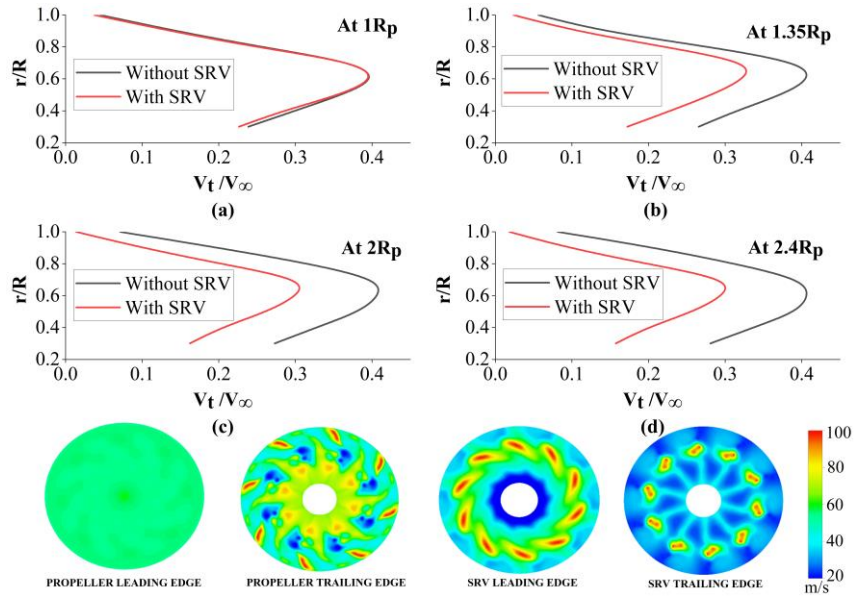

Fig. 10 Radial Distribution and Profile Transformation of Tangential Velocity at 0° SRV Pitch

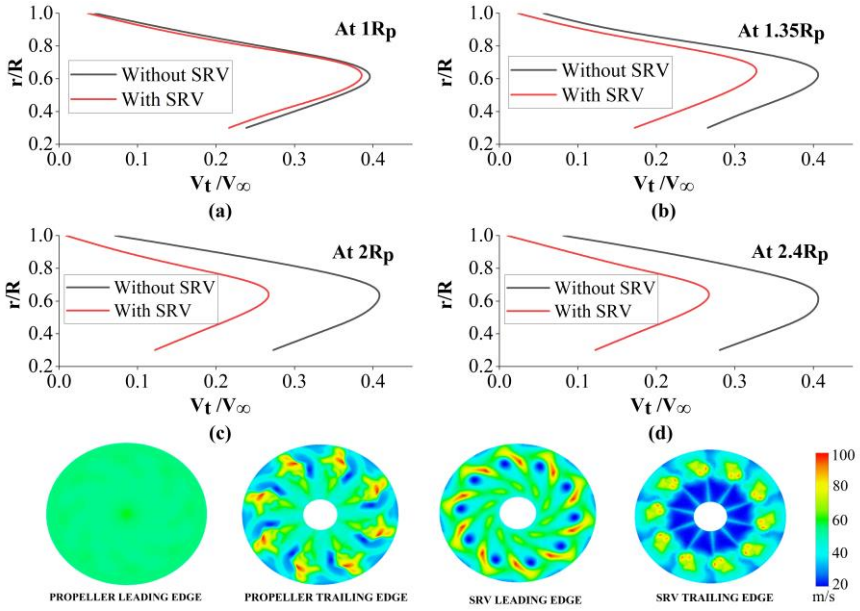

Fig. 11 Radial Distribution and Profile Transformation of Tangential Velocity at 5° SRV Pitch

exhibits a relatively high tangential velocity due to the propeller's swirl, but as the flow moves through the SRV at 5°, the reduction in tangential velocity is less pronounced. At $1.35R_p$, the tangential velocity decreases by approximately 7-10%, as the SRV begins to redirect some of the tangential energy into axial motion. The SRV's 5° pitch angle is not as effective at recovering tangential energy as the 10° pitch, so the reduction in tangential velocity is more gradual.

Downstream, near the SRV trailing edge at 2Rp, the tangential velocity continues to decrease, but at a slower rate than at 10°. The reduction is around 10-15%, reflecting a moderate transformation of the tangential component into axial energy. As the flow moves to 2.4Rp, the tangential velocity decreases further, showing a reduction of approximately 12-17%. Although the 5° pitch angle still reduces tangential velocity, the transformation is less efficient compared to the higher pitch angle, and the flow remains somewhat swirl-dominated, though more aligned with the axial direction than in the baseline case.

Profile transformation contours show that at the SRV's leading edge, the tangential velocity is still significant, though slightly reduced compared to the 10° case. The reduction in tangential velocity becomes more noticeable as the flow passes through the SRV blades, but the conversion of tangential energy into axial motion is less complete, resulting in a higher tangential velocity at the SRV's trailing edge compared to the 10° pitch case.

Case 3: SRV at a Pitch = 10°

Figure 12 presents the time averaged tangential velocity distribution at the four tangential planes for the

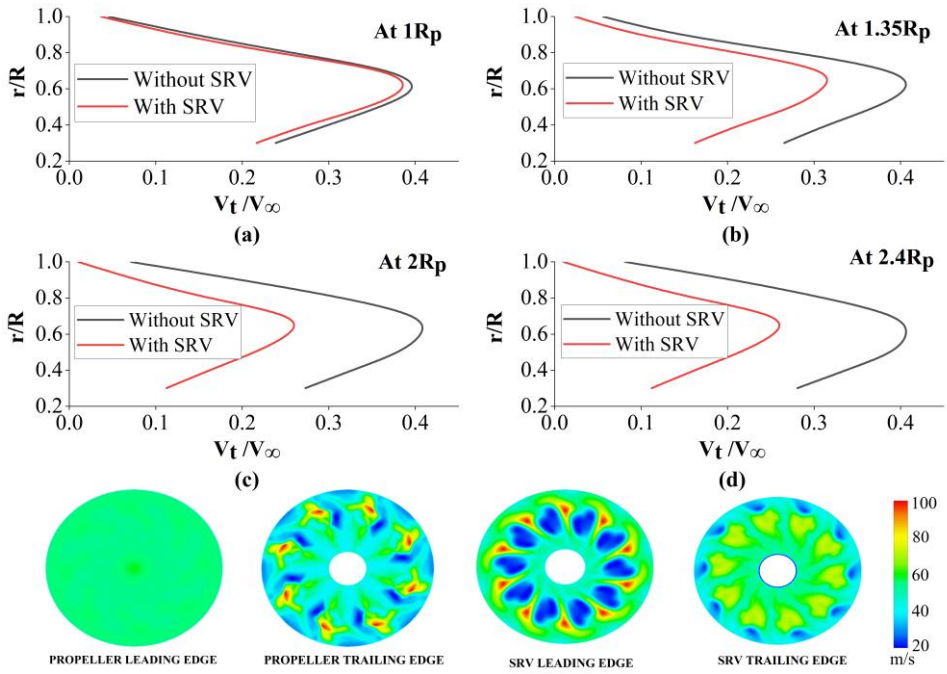

Fig. 12 Radial Distribution and Profile Transformation of Tangential Velocity at 10° SRV Pitch

normalized radial locations for the ten-degree pitch. Additionally, the profile transformation contours for tangential velocity at the propeller's leading edge & trailing edge, SRV's leading edge & trailing edge, are also shown.

When the SRV set at a 10° pitch angle, the tangential velocity undergoes a significant reduction compared to the baseline case (without SRVs). Upstream, at $1R_p$, the flow exhibits substantial tangential motion due to the rotational energy imparted by the propeller. The propeller blades generate a strong swirl, leading to a high tangential velocity. However, as the flow passes through the SRV at 10°, the tangential component is reduced as the SRV blades convert some of the tangential energy into axial energy. At $1.35R_p$, the tangential velocity decreases noticeably as the swirl is progressively dampened. The SRV effectively redirects the flow towards the axial direction, reducing the tangential component by approximately 10-12% compared to the upstream planes.

Downstream, near the SRV's trailing edge at $2R_p$, the tangential velocity continues to decrease as the SRV blades efficiently recover tangential energy and redirect it into axial motion. At $2R_p$, the tangential velocity has reduced by around 15-20%, reflecting the SRV's role in mitigating the swirl. Moving further downstream to $2.4R_p$, the tangential velocity continues to decrease, showing a reduction of approximately 18-22%. The 10° SRV pitch angle is the most efficient at converting tangential energy into axial kinetic energy, resulting in the lowest tangential velocity downstream, and the flow becomes more uniform and aligned with the thrust axis.

The profile transformation contours for tangential velocity reveal that at the SRV's leading edge, the tangential velocity is still high, reflecting the residual swirl from the propeller. As the flow passes through the SRV blades, the tangential component decreases, and by the time it reaches the SRV's trailing edge, the tangential velocity is at its minimum. This indicates the effective conversion of tangential energy into axial kinetic energy by the 10° pitch SRV, enhancing the overall system efficiency.

Swirl Angle

Case 1: SRV at a Pitch = 0°

Figure 13 presents the time averaged swirl angle distribution at the four axial planes of $1R_p$, $1.35R_p$, $2R_p$ and $2.4R_p$ plotted against the normalized radial locations. With the SRV set at a 0° pitch angle, the reduction in swirl angle is minimal, and the swirl component remains largely unaffected. Upstream, at $1R_p$, the swirl angle is high due to the strong swirl generated by the propeller. As the flow moves to $1.35R_p$, there is a slight decrease in the swirl angle as the propeller imparts some axial thrust, but the overall swirl remains significant. The SRV at 0° pitch does little to alter the flow's rotational component, so the swirl angle remains high, with only a small reduction of around 3-5%.

Downstream at $2R_p$, the swirl angle remains relatively high, with a slight reduction of approximately 5-7%. The SRV at 0° pitch does not effectively mitigate the swirl, and the tangential energy remains largely unconverted into axial motion. At $2.4R_p$, the swirl angle decreases slightly more, but only by about 7-9%, showing the inefficiency of the 0° pitch SRV in reducing swirl. This results in a flow that is still somewhat swirl-dominated and less aligned with the thrust axis compared to the higher pitch angle cases.

Case 2: SRV at a Pitch = 5°

From Fig. 14, at a 5° pitch angle, the SRV still reduces the swirl angle, but the effect is less pronounced than at 10°. Upstream, at $1R_p$, the swirl angle is still high due to

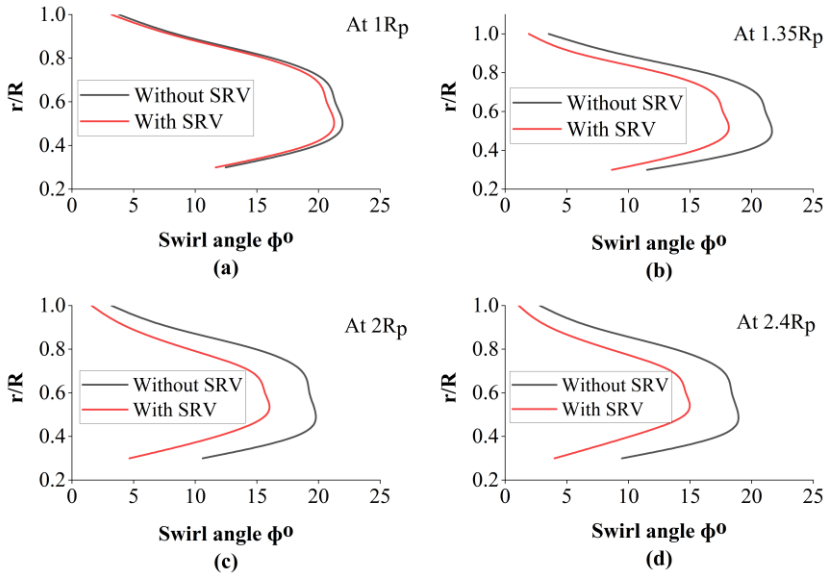

Fig. 13 Radial distribution of the swirl angle component downstream of the propeller designed for SRV at a pitch of 0° at four different planes

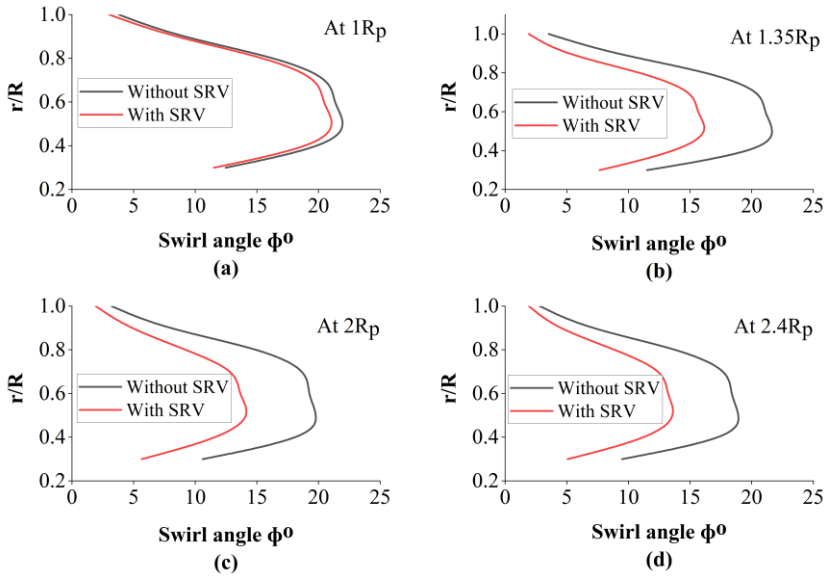

Fig. 14 Radial distribution of the swirl angle component downstream of the propeller designed for SRV at a pitch of 5° at four different planes

the propeller-induced swirl. As the flow moves downstream to $1.35R_p$, the swirl angle begins to decrease as the propeller generates axial thrust, but the reduction is modest compared to the 10° pitch case. The swirl angle is reduced by approximately 8-10%, as the SRV at 5° pitch starts to redirect some of the tangential energy into axial motion, though not as effectively as the higher pitch angle.

Downstream at $2R_p$, the swirl angle continues to decrease, but the reduction is less pronounced than at 10°. The swirl angle is reduced by around 15-18%, reflecting the SRV's ability to mitigate the swirl, although the conversion of tangential energy into axial energy is less efficient. Moving further downstream to $2.4R_p$, the swirl angle continues to decrease by approximately 18-22%, but the overall reduction is smaller than at the 10° pitch. This indicates that while the 5° SRV pitch helps in reducing swirl, the effect is more gradual and less complete compared to the 10° pitch angle.

Case 3: SRV at a Pitch = 10°

Figure 15 presents the time averaged swirl angle distribution at the two planes downstream of the propeller and two planes downstream of the SRV for the normalized radial locations for the ten-degree pitch.

At a 10° pitch angle, the SRV plays a crucial role in significantly reducing the swirl angle, which is a measure of the rotational component of the flow. Upstream, at $1R_p$ (one propeller radius downstream from the rotor), the swirl angle is relatively high due to the strong swirling motion imparted by the propeller blades. The propeller

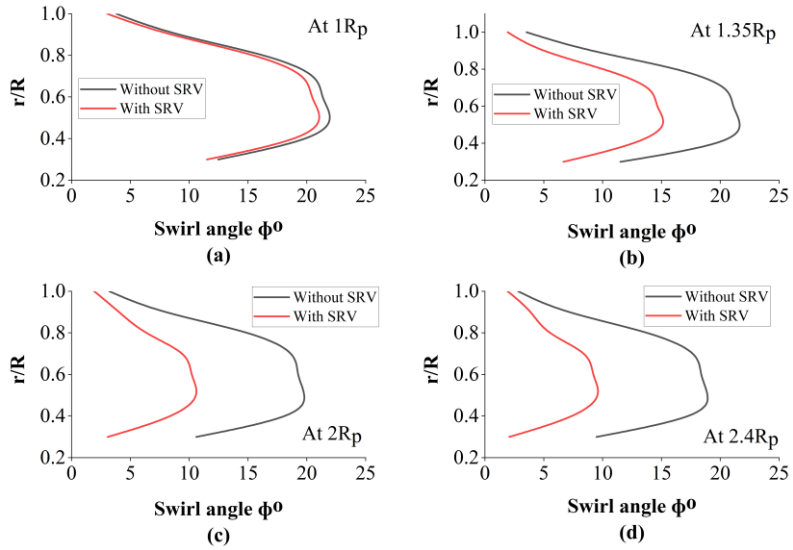

Fig. 15 Radial distribution of the swirl angle component downstream of the propeller designed for SRV at a pitch of 10° at four different planes

generates a substantial tangential velocity, resulting in a high swirl angle. As the flow moves to the propeller's trailing edge at $1.35R_p$, the swirl angle remains elevated, though slightly reduced compared to the rotor plane, as the propeller begins to impart axial thrust, which diminishes the swirl to some extent.

With the introduction of the SRV at 10° pitch, the swirl angle is effectively reduced. As the flow passes through the SRV blades, the tangential velocity is converted into axial velocity, and the swirl is mitigated. At $1.35R_p$, the swirl angle is reduced by approximately 12-15%, reflecting the SRV's ability to redirect the flow and dampen the rotational component. Moving downstream, at $2R_p$ (two propeller radii downstream from the rotor trailing edge), the swirl angle is significantly lower due to the SRV's efficient conversion of tangential energy. The swirl angle at $2R_p$ is reduced by around 20-25%, showcasing the effectiveness of the 10° SRV pitch in transforming the swirling flow into more axial motion. By the time the flow reaches $2.4R_p$, the swirl angle is further reduced by approximately 25-30%. This reduction in swirl angle is essential for improving the overall system efficiency, as it leads to a smoother, more uniform flow that aligns with the thrust axis. Efficiency generally increases with pitch angle due to more effective swirl recovery. Therefore, excessive pitch angles (such as 10°) introduce more flow deflection, increasing the overall efficiency compared to lower pitch angles.

4.2. Unsteady Axial Velocity and Static Pressure Distribution

The present investigation is unsteady computational analysis of the isolated propeller and propeller-SRV configurations. Figure 16 shows the distribution of unsteady static pressure and Fig. 17 presents the distribution of unsteady static pressure ($P^{'}/P_{\infty}$) normalized by freestream pressure for the ten-degree pitch for one blade passing period. Figure 18 presents the distribution of unsteady axial velocity normalized by freestream

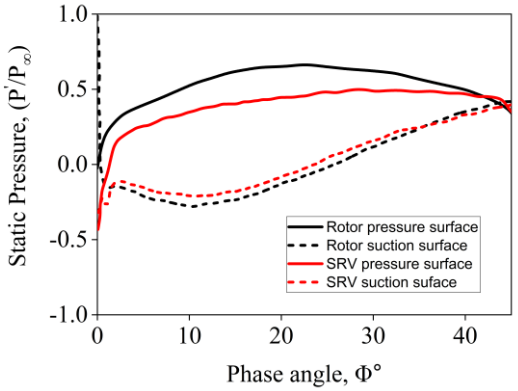

Fig. 16 Unsteady static pressure distribution of propeller and SRV at 95% of the blade span at 10° pitch for one blade passing period

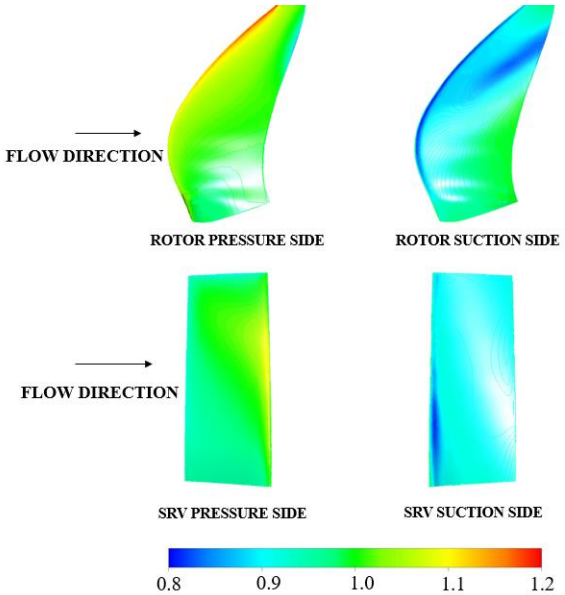

Fig. 17 Static pressure ($P^{'}/P_{\infty}$) on the suction and pressure side of Rotor-SRV designed for a pitch of 10° for one blade passing period

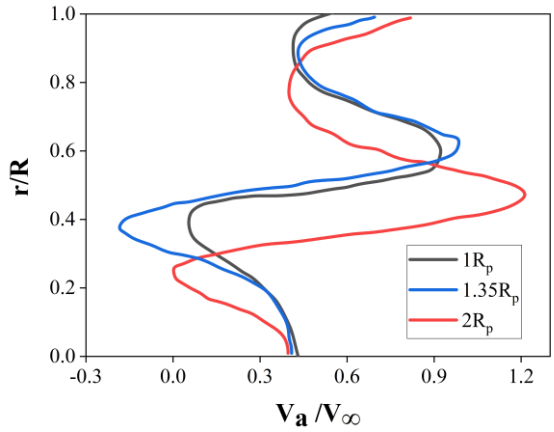

Fig. 18 Unsteady axial velocity distribution of propeller and SRV at the wake distance of 1.35R_p and 2R_p at 10° pitch for one blade passing period

velocity at three axial locations of 1R_p, 1.35R_p and 2R_p for the ten-degree pitch for one blade passing period.

From Fig.16, the unsteady static pressure distribution at 95% of the blade span highlights the impact of SRVs on flow dynamics near the blade surface, where interactions between the rotor and SRVs are most significant. At this region, the pressure differential between the suction and pressure sides at the blade tip, strongly influence the flow. The unsteady nature of the flow at the blade tip results in cyclic pressure changes during one blade-passing period. The SRV placement at a 10° pitch reduces the swirling flow, thereby influencing the static pressure distribution.

From Fig.17, the distribution of unsteady static pressure normalized by freestream pressure on the suction and pressure sides of both the rotor and SRV blades are shown over one blade-passing period. These variations are influenced by the rotor-SRV configuration at a 10° pitch. The fluctuating pressure difference across the suction and pressure sides is cyclic, dictated by the blade-passing frequency and the SRV's impact on the flow field. The

SRV modifies the pressure distribution by altering the swirl recovery process, affecting the pressure difference on both blade sides. This influence is particularly noticeable in the regions near the blade tip, where the pressure differential fluctuates the most due to the interaction of tip vortices and SRV-induced flow straightening.

From Fig.18, the unsteady axial velocity normalized by freestream velocity downstream of the rotor and SRV is illustrated at 1R_p, 1.35R_p, and 2R_p, showing the transient characteristics influenced by blade-passing effects and the wake recovery process.

At 1R_p and 1.35R_p downstream of the rotor (between rotor and SRV):

The axial velocity exhibits periodic variations due to the rotor's blade-passing frequency. High-velocity peaks occur near the mid-span, where the blade accelerates the flow, while low-velocity troughs are observed near the hub due to wake effects. These velocity fluctuations shift angularly over time, creating a phase-lagged pattern synchronized with the blade-passing period. At these distances, the wake begins to diffuse, but sharp oscillations persist, reflecting the rotor's influence on the flow.

At 2R_p downstream of the rotor (after SRV):

The axial velocity profile demonstrates significant improvements due to the flow-straightening effect of the SRVs. By reducing tangential velocity and converting swirl into axial flow, the SRVs create a more uniform axial velocity distribution. The wake recovery process is evident, particularly near the hub, where velocity deficits are mitigated. While residual periodic variations remain due to incomplete damping of blade-passing effects, the SRVs attenuate these oscillations, especially at mid-span and near the tip regions, where the flow energy is higher.

The overall wake recovery process reflects the combined effects of the rotor and SRVs. The rotor introduces axial and tangential velocity components, creating a non-uniform wake. The SRVs counteract the swirl, redistribute wake energy, and improve axial velocity uniformity while damping oscillations downstream. At 1.35R_p, sharp fluctuations dominate due to the rotor's influence, but at 2R_p downstream of the SRV, the flow achieves greater uniformity, underscoring the SRVs' effectiveness in enhancing propulsive efficiency and minimizing velocity deficits in the propeller wake system.

5. CONCLUSION

The integration of SRVs downstream of propeller presents a promising path for improving propulsive efficiency in aircraft configurations. Numerical simulation comparing propeller with and without SRVs, particularly in tractor configuration, has revealed significant potential for enhancing propulsive efficiency. The computational analysis has been conducted to comprehensively understand the aerodynamic effects and performance enhancements of the propeller – SRV configuration.

The analysis shows that increasing the SRV pitch angle from 0° to 10° significantly improves aerodynamic performance. At 10°, the axial velocity is the highest, while tangential velocity and swirl angle decrease, reflecting effective swirl recovery and reduced wake rotation. Static pressure recovery also improves with higher pitch angles contributing to better propulsion efficiency. The rotor stator interaction effect is significant in terms of axial velocity increase brought out clearly from by the transient analysis. Overall, a 10° SRV pitch demonstrates the best performance for the present eight bladed propeller and ten bladed SRV configuration, confirming its effectiveness in converting rotational losses into useful thrust and enhancing the propeller-SRV efficiency. The inclusion of SRVs amplifies swirl recovery effects, leading to enhanced axial flow speed and overall efficiency gains. The vane design with ten-degree pitch could increase the propeller efficiency by approximately 3.25% and the overall efficiency of the propeller – SRV combination improved by 3.46 %.

The inclusion of SRVs led to a significant increase in thrust and torque, with an increase in thrust of 23N for 10° pitch and an increase in torque of 5.25Nm for 5° pitch,

respectively, compared to the isolated propeller. Further, 4.46% increase in the power coefficient is attained for SRV with ten-degree pitch.

Continued research focusing on improving the SRV design in terms of blade profile, twist and the number of vanes is expected to lead to the optimum configuration that provides the best overall performance in terms of thrust and overall efficiency of the rotor - SRV combination.

ACKNOWLEDGEMENTS

The authors would like to thank Hindustan Institute of Technology and Science for the support extended to the present research work. The authors would also like to thank their colleagues for the insightful discussions.

CONFLICT OF INTEREST

On behalf of all authors, the corresponding author states that there is no conflict of interest.

AUTHORS CONTRIBUTION

R. Santhi (Corresponding author): Data curation (lead); Formal analysis (lead); Investigation (equal); Validation (lead); Writing – original draft (lead).
P. Vasanthakumar: Conceptualization (lead); Formal analysis (equal); Resources (equal); Supervision (equal); Writing – review & editing (equal).

REFERENCES

ANSYS® (2013). Academic research release 15.0. Help system. ANSYS Mechanical Element Reference.

ATR (2018). Connecting the Future, Turboprop Market Forecast 2018–2037.

Beaumier, P. (2012, September). *Numerical tools developed at onera for the aerodynamic assessment of propellers and counter-rotating open rotors.* 28th Congress of the International Council of the Aeronautical Sciences, Brisbane (Vol. 74, p. 99).

Beck, N., Radespiel, R., Lenfers, C., Friedrichs, J., & Rezaeian, A. (2015). Aerodynamic effects of propeller slipstream on a wing with circulation control. *Journal of Aircraft*, *52*(5), 1422–1436. https://doi.org/10.2514/1.C032901

Dittmar, J. H., & Hall, D. G. (1990). *The effect of swirl recovery vanes on the cruise noise of an advanced propeller.* 13th Aeroacoustics Conference, AIAA Paper 1990-3932, Oct. 1990. https://doi.org/10.2514/6.1990-3932

Gazzaniga, J., & Rose, G. (1992). *Wind tunnel performance results of swirl recovery vanes as tested with an advanced high-speed propeller.* 28th Joint Propulsion Conference & Exhibit, 1992, Nashville, TN, USA. https://doi.org/10.2514/6.1988-3152

Hager, R. D. (1988). *Advanced turboprop project* (Vol. 495). Scientific and Technical Information Division, National Aeronautics and Space Administration.

International Air Transport Association. (2018). Future of the airline industry 2035. https://www. iata. org/policy/Documents/iata-future-airline-industry. pdf.

International Civil Aviation Organization, "ICAO Environmental Report 2016". http://www.icao.int/environmental-protection/Documents/ICAO%20Environmental%20Report%202016.pdf.

Kroo, I. (1986). Propeller-wing integration for minimum induced loss. *Journal of Aircraft*, *23*(7), 561-565. https://doi.org/10.2514/3.45344

Lombardi, L. (2011, May). *ATR, program review and market outlook.* 10th EWADE Conference, Naples.

Mikkelson, D. C., Mitchell, G. A., Bober, L. J. (1984). *Summary of recent NASA Propeller Research*. NASA Technical Memorandum 83733.

Miller, C. J. (1988, July). *Euler analysis of a swirl recovery vane design for use with an advanced single-rotation propfan.* AIAA/SAE/ASME/ASEE 24th Joint Propulsion Conference, AIAA Paper 1988-3152. https://doi.org/10.2514/6.1988-3152

Miranda, L., & Brennan, J. (1986, June). *Aerodynamic effects of wingtip-mounted propellers and turbines*. 4th Applied Aerodynamics Conference (P. 1802). https://doi.org/10.2514/6.1986-1802

Ortun, B., Boisard, R., & Gonzalez-Martino, I. (2012). *In-plane airloads of a propeller with inflow angle: prediction vs. experiment*. 30th AIAA Applied Aerodynamics Conference, New Orleans, Louisiana, 25–28 June, American Institute of Aeronautics and Astronautics. https://doi.org/10.2514/6.2012-2778

Rohrbach, C., Metzger, F. B., Black, D. M., & Ladden, R. M. (1982). Evaluation of wind tunnel performance testings of an advanced 45 deg swept 8-bladed propeller at Mach numbers from 0.45 to 0.85 (No. NASA-CR-3505). NASA.

Samuelsson, I. (1990). *Experimental investigation of low-speed model propeller slipstream aerodynamic characteristics including flow field surveys and nacelle/wing static pressure measurements.* ICAS, Congress, 17 th, Stockholm, Sweden (pp. 71-84).

Santhi, R., & Vasanthakumar, P. (2022). Computational fluid dynamics for turbomachinery technologies with a focus on high-speed rotor blades. *Materials Today: Proceedings.* https://doi.org/10.1016/j.matpr.2022.08.555.

Sinnige, T., van Kuijk, J. J., Lynch, K. P., Ragni, D., Eitelberg, G., & Veldhuis, L. L. (2015). The effects of swirl recovery vanes on single-rotation propeller aerodynamics and aeroacoustics. In 21st AIAA/CEAS Aeroacoustics Conference (p. 2358). https://doi.org/10.2514/6.2015-2358

Stefko, G. L., & Jeracki, R. J. (1985). *Wind-tunnel results*

of advanced high-speed propellers at takeoff, climb, and landing mach numbers (No. NASA-TM-87030).

Stokkermans, T. C. A. (2015). *Design and analysis of swirl recovery vanes for an isolated and a wing mounted tractor propeller.* Delft University of Technology Master Thesis.

Stokkermans, T. C. A., Van Arnhem, N., & Veldhuis, L. L. M. (2016, July). *Mitigation of propeller kinetic energy losses with boundary layer ingestion and swirl recovery vanes.* Proceedings of the 2016 Applied Aerodynamics Research Conference, Royal Aeronautical Soc., London (pp. 56-69).

Strack, W. C., Knip, G., Weisbrich, A. L., Godston, J., & Bradley, E. (1981). *Technology and benefits of aircraft counter rotation propellers* (No. E-1414).

Stuermer, A. W. (2006, 9–12 July). *Unsteady CFD simulations of propeller installation effects*. 42nd AIAA/ASME/SAE/ASEE Joint Propulsion Conference and Exhibit, Sacramento, California, American Institute of Aeronautics and Astronautics. https://doi.org/doi:10.2514/6.2006-4969

Stuermer, A. W., & Akkermans, R. A. (2014a). *Validation of aerodynamic and aeroacoustic simulations of contra-rotating open rotors at low-speed flight conditions.* 32nd AIAA applied aerodynamics conference (p.3133). https://doi.org/10.2514/6.2014-3133

Stuermer, A. W., Spinner, S., Trost, M., & Schnell, R. (2022). *Aerodynamic analysis of a transport aircraft with a boundary layer ingesting aft-propulsor at cruise flight conditions.* AIAA Aviation 2022 Forum (p. 3301). https://doi.org/10.2514/6.2022-3301

Stuermer, A., Yin, J., & Akkermans, R. (2014b). Progress in aerodynamic and aeroacoustic integration of CROR propulsion systems. *The Aeronautical Journal*, *118*(1208), 1137-1158. https://doi.org/10.1016/j.cja.2014.03.009

Stürmer, A., & Akkermans, R. A. (2014c). Multidisciplinary analysis of CROR propulsion systems: DLR activities in the JTI SFWA project. *CEAS Aeronautical Journal*, *5*(3), 265-277. https://doi.org/10.1007/s13272-014-0105-4

van Kuijk, J. J. A. (2015). *Analysis of swirl recovery vanes: propulsion system performance and slipstream-wing interaction* [Master's thesis, Aerospace Engineering, Delft University of Technology]. https://resolver.tudelft.nl/uuid:33cc26ac-2e9b-4bd5-a5dc-55756db1f863

Veldhuis, L. L. M. (2005). Propeller wing aerodynamic interference [Ph.D. Dissertation, Dept. of Aero-space Engineering, Delft Univ. of Technology], Delft, The Netherlands. https://resolver.tudelft.nl/uuid:8ffbde9c-b483-40de-90e0-97095202fbe3

Wang, Y., Li, Q., Eitelberg, G., Veldhuis, L. L. M., & Kotsonis, M. (2014). Design and numerical investigation of swirl recovery vanes for the Fokker 29 propeller. *Chinese Journal of Aeronautics*, *27*(5), 1128-1136. https://doi.org/10.1016/j.cja.2014.03.009

Witkowski, D. P., Lee, A. K., & Sullivan, J. P. (1989). Aerodynamic Interaction Between Propellers and Wings. *Journal of Aircraft*, *26*(9), 829–836. https://doi.org/10.2514/3.45848

Yamamoto, O. (1992). *Numerical calculations of propfan/swirl recovery vane flow field.* 28th Joint Propulsion Conference and Exhibit (p. 3771). https://doi.org/10.2514/6.1992-3771